Deposition and Aggregation of Brownian Particles in Trickle-Bed Reactors

Ion Iliuta and Faïçal Larachi
Chemical Engineering Dept., Laval University, Quebec G1K 7P4, Canada

DOI 10.1002/aic.11023
Published online October 16, 2006 in Wiley InterScience (www.interscience.wiley.com).

When dilute liquid suspensions contaminated with Brownian fine solids are treated in catalytic trickle-bed reactors, bed plugging develops and increases the resistance to two-phase flow until ultimate unit shutdown for bed substitution with pristine catalyst is imposed. One of the important aspects during plugging with Brownian particles is the aggregation of fines and the release of the fine particles and aggregates from pore bodies within the porous bed as a result of the hydrodynamic or colloidal forces. Current physical models linking gas–liquid flow to the filtration process in high-pressure/temperature trickle beds neglect the possible colloidal particle aggregation and the release of aggregates. This work attempts to fill this gap by developing a Euler–Euler fluid dynamic model based on the volume average mass, momentum, and species balance equations, filtration equations for the Brownian particles and the aggregates, and the discrete population balance equations for the agglomeration of particles. Both monolayer and multilayer depositions were considered for Brownian particles and only the monolayer deposition in the case of the detaching aggregates. The release of fine particles and aggregates from the collector surface was assumed to be induced by the colloidal forces in the case of Brownian particles/aggregates or by the hydrodynamic forces in the case of non-Brownian aggregates. Brownian particle aggregation was described by the rate at which a certain size aggregate is being formed by smaller aggregates less the rate at which the aggregate combines to form a larger aggregate.
 AIChE J, 52: 4167–4180, 2006
Keywords: trickle beds, two-phase flow, plugging, deposition, aggregation, release

Introduction

Oil refining industrial practices are continually changing. These changes are imposed either because of the quality of the feeds or because of the standards the manufactured products must meet.[1] Catalytic hydrotreating, a key process in petroleum refining, is used to enhance the quality of residue or distillate streams by selectively removing the objectionable S, N, and O heteroatoms in the form of H_2S, NH_3, and H_2O through, respectively, hydrodesulfurization, hydrodenitrogenation, and hydrodeoxygenation reactions. In actual industrial practice, depending on the oil fraction boiling point range, hydrotreating takes place either as a gas–solid or a three-phase process. Because hydrotreating reactions are usually irreversible, the reaction temperature is constrained by the required reaction rate and catalyst tolerance to deactivation.[2] Such reaction temperature typically lies in the range 573–653 K, where often the reactions with high boiling point heavy fractions are carried out in three-phase trickle-bed reactors.[3,4]

Although the main focus of hydrotreaters is on heteroatom removal, feed streams can also contain a variety of fine solid particles including clays entrained during distillation, coke particles from upstream delayed cokers, corrosion products, and other minerals.[5–7] These fine particles can deposit in the catalyst bed, leading to porosity reduction and thus to bed

Correspondence concerning this article should be addressed to F. Larachi at faical.larachi@gch.ulaval.ca.

plugging. The cumulative effect of several daily thousands of barrels of treated feeds irremediably turns hydrotreaters into giant filters. Accumulation of fine particles in the catalyst bed alters both the geometry of the bed interstices and the nature of the collector (catalyst particle) surfaces. Such changes translate in an increased reactor pressure gradient until eventually the unit is prematurely shut down for the catalyst to be replaced.[6]

Studies of Brownian particle deposition in packed beds tend to support the contention that the deposition can be considered to involve two sequential processes: a transport process and an attachment process.[8,9] The transport process brings a particle from the bulk liquid to very near the surface of the collector and the attachment process binds the two surfaces together in some way. Convection, diffusion, and gravity dominate the transport step and colloidal interactions between the interacting surfaces usually control the attachment step. London–van der Waals and double-layer forces are frequently used to describe the attachment process. The former is attractive and remains essentially constant during deposition. The double-layer force can be either attractive or repulsive and may change during deposition. The existence of repulsive double layers can also result in the exclusion of certain areas on the collector surface from particle deposition because of electrical repulsion, which is referred to as the excluded surface effect.[10] Exclusion of certain areas on the collector surface may also result from collector surface heterogeneity. Particle deposition occurs only at those sites displaying favorable interactions, whereas the other parts that exhibit unfavorable interactions do not allow deposition.[10] However, intermingling between the hydrodynamics, the fine–collector, and fine–fine surface interactions and the physicochemical mechanisms developing inside the porous bed makes the fundamentals of the deposition process difficult to grasp.

Numerous investigators in the past have attempted to describe the transient behavior of the deposition process, at both macroscopic and microscopic levels, in the case of single-phase flow through porous media. The macroscopic studies are aimed at the phenomenological description of the deposition process, the prediction of its dynamic behavior, and the development of methodology and techniques for design, calculation, and optimization. Microscopic approaches, known as trajectory theories, are intended to provide information and insight about the mechanisms of particle deposition, the conditions under which deposition may be facilitated, and the effect of deposition on the structure of packed-bed media. The phenomenological theory of deposition has two shortcomings: the lack of generality and the failure to provide a fundamental understanding of the mechanism of deposition. Conversely, a trajectory theory examines the deposition of each particle on the collector as suspension flows through the collector. Even if current trajectory analysis models differ by their geometrical representation of the granular media and inclusion of surface forces there is a little difference in the accuracy between them.[11] Trajectory analysis, however, applies only to the initial stage of deposition. To model the deposition process in its entirety, the effect of deposited particles on collector efficiency must be calculated. With deposited particles on collector surfaces, the surface interactions between the collecting body and particles to be collected become more complicated. If particle–particle interactions are favorable the deposition rate increases in time because deposited particles act as additional deposition sites. In the presence of unfavorable surface interactions deposition rates may be a fraction of those under favorable surface interactions, even if all other conditions are the same.[10]

In contrast, the literature still remains rather scanty with respect to the complex hydrodynamics and surface phenomena involved in the plugging with fine particles of packed-bed gas–liquid–solid reactors despite the critical operational problem of fines in the petroleum refining industry. Thus, a limited number of experimental works on the process of fines accumulation[6,7,12,13] and only some attempts concerning the modeling and conceptualization of fines deposition dynamics have been reported.[14–19] The few available experimental studies showed that the pressure drop increases monotonically with the concentration of fine particles and this increase correlates well with the reduction in effective porosity arising from the accumulation of fines. All the experimental studies suggest that the major change resulting from the deposition of fine particles involves the effective size and geometry of catalyst particles, the surface characteristics of the catalyst particles, the local porosity, and the effective porosity of the bed.

One of the important aspects during plugging with Brownian particles is *aggregation* of fines and *release* of fine particles and aggregates from pore bodies within the porous bed resulting from the hydrodynamic or colloidal forces. The aggregations of fines and detachment of deposited fine particles and aggregates or inhibition of detached aggregates deposition process over some regions of the catalytic collectors have not received attention in the trickle bed literature. Aggregation involves the formation of assemblies of particles brought together by collisions and held in contact by surface forces.[20] Two distinct, limiting regimes of irreversible colloid aggregation have been identified.[20] Diffusion-limited colloid aggregation occurs when there is no repulsive force between the colloidal particles so that the aggregation rate is dependent solely on the time taken for particles (or aggregates) to encounter each other by diffusion. The aggregates themselves continue to diffuse, collide, and form larger aggregates. In the regime of reaction-limited aggregation, additional repulsive forces caused by electrostatic forces or steric hindrance prevent the particle from coagulating. The foundational work for our understanding today of the process of particle aggregation in fluids is a result of research traced back to 1917 by von Smoluchowski,[21] who considered particle aggregation to be equivalent to a series of chemical reactions, and developed equations describing particle aggregation rates as well as expressions for the rate of particle collisions in solution. The release of non-Brownian aggregates is a threshold process, that is, a minimum perturbation (critical hydrodynamic stress) is required to detach the aggregate from the pore surface.[22,23] On the other hand, the release of colloidal particles or colloidal aggregates from the collector surface is controlled by the colloidal forces. The released particles or aggregates while flowing with the liquid phase can either readhere to the collector surface, flow without capture, or become entrapped at the pore constrictions. A limited number of experimental works on the detachment of particles[24–28] and only some attempts

concerning the modeling and conceptualization of detachment dynamics of particles[26,27,29,30] have been reported.

Currently, physical models linking gas–liquid flow to the filtration process in trickle beds neglect the possible colloidal particle *aggregation* and *release* of aggregates and fine particles.[14–16,19] An attempt was thus made in the present study in which the authors sought to develop a Euler–Euler fluid dynamic model based on the volume average mass, momentum, and species balance equations, filtration equations for the Brownian particles and the aggregates, and the discrete population balance equations for the agglomeration of particles. Both monolayer and multilayer depositions were considered for Brownian particles and only monolayer deposition in the case of the detached aggregates. Release of the fine particles or aggregates from the collector surface was supposed to be induced by the colloidal forces in the case of Brownian particles/aggregates or by the hydrodynamic forces in the case of non-Brownian aggregates. Brownian particle aggregation was described by the rate at which a certain size aggregate is being formed by smaller aggregates less the rate at which the aggregate combines to form a larger aggregate (population balance equations of von Smoluchowski[21]). Coupling between the liquid suspension and solids was monitored by the fines and aggregates filtration rate equation; the fines and aggregates release rate equations and the interaction drag or momentum exchange force terms.

Governing equations for deposition and aggregation of Brownian particles in trickle-bed reactors

A cocurrent two-phase trickle flow through a porous medium of uniform initial porosity ε^o and single-sized catalytic particles is considered. For each flowing phase, we shall assume unidirectional, isothermal, incompressible, viscous Newtonian, and passive (no chemical reaction) conditions. The gas/liquid/Brownian particles/aggregates/porous medium multiphase system is viewed as a system of three interpenetrated continua:

(1) A flowing gas phase

(2) A dilute pseudo-homogeneous suspension phase consisting of the liquid, the seeding primary Brownian particles, and the detached aggregates, referred to hereafter as *fluid*

(3) A stationary pseudo-continuous solid phase made up of the packing particles—also referred to as *collectors* in this work—constituting the clean porous medium as well as of the Brownian particles and the aggregates that become captured/generated onto their surface.

Further assumptions inherent to the formulation developed here are:

- The fluid properties, such as density, viscosity, and holdup, are equal to those of the embracing liquid (inlet Brownian particles volume fraction usually down to 0.1‰).
- The bed is partially wetted by the liquid phase.
- Two-phase flow is annular and completely separated.

Each phase, that is, gas, liquid, and solid, behaves as a continuum so that the macroscopic differential balance equations can be applied; however, except for the solid mass conservation, the solid stress balance is not included in the present analysis.

Variations of concentrations of Brownian particles and aggregates and other quantities are significant only in the major flow direction, that is, the streamwise axial direction here.

Only the inlet liquid was considered as a source for Brownian particles without considering fines generated in the catalyst bed (attributed to attrition, byproduct buildup, etc.). The aggregates (assemblies of Brownian particles) are generated in the catalyst bed.

Only the deposition under favorable conditions of surface interactions was considered (the double-layer force is attractive). The influence of the gas phase on the deposition process of Brownian particles and aggregates was neglected.

The generation of aggregates was considered to take place by collision and subsequent bonding of primary Brownian particles transported from the bulk liquid to the surface of the collector in the liquid approaching the collector (the transport to the grain surface is quantified by the collection efficiency). The fine–fine attractive interactions within the bulk liquid phase are assumed absent or at least small enough to preclude aggregation. Fracturing of the agglomerates by the disruptive stresses created by the liquid and gas motion was neglected.

The primary Brownian particles seeded in the liquid are considered single-sized with density ρ_f and diameter d_f. The aggregates are formed by lumps of primary particles (or monomers).

The gas–liquid interface is impervious to the Brownian particles and aggregates. Migration of Brownian particles and aggregates to the gas–liquid interface caused by fine surface properties (akin to froth flotation in mineral processing) has been neglected in the present analysis. The importance of such migration of fines and aggregates in trickle-bed flows is still to be elucidated as well as the criteria to be used to identify whether it is important.

Another issue relates to size and wettability (or contact angle) of Brownian particles and aggregates, which may be important and which was also neglected in the present development.

The net sink in the fluid momentum balance resulting from the mass transfer of Brownian particles and detached aggregates from the fluid to the collector is negligibly small.

Bed plugging by the blocking and the sieving modes does not take place.[31,32]

The release of Brownian particles or aggregates ($d_f < 2$ μm) from the collector surface is controlled by the colloidal forces (Brownian diffusion through the hydrodynamic boundary layer in the absence of energy barrier).[22,28]

The detachment of non-Brownian aggregates ($d_f > 2$ μm) is induced by hydrodynamic forces.[28]

The Euler–Euler model is based on the volume-averaged form of the transport equations developed for multiphase systems[33] and the population balance equations for the agglomeration of particles.[21] The general model equations consist of the conservation of volume, the continuity, and the Navier–Stokes equations for the gas and the fluid phases; the continuity equation for the solid stationary phase; the species balance equation for the Brownian particles and detached aggregates undergoing migration from the fluid phase to the solid phase; and filtration equations for the Brownian particles and aggregates:

Conservation of Volume

$$\varepsilon_g + \varepsilon_l = \varepsilon \tag{1}$$

Continuity Equations for the Gas, the Fluid, and the Solid Phases

$$\frac{\partial}{\partial t}(\varepsilon_g \rho_g) + \frac{\partial}{\partial z}(\varepsilon_g \rho_g u_g) = 0 \tag{2}$$

$$\frac{\partial}{\partial t}(\varepsilon_l \rho_l) + \frac{\partial}{\partial z}(\varepsilon_l \rho_l u_l) = -\rho_f \frac{d\sigma}{dt} \tag{3}$$

$$\frac{\partial}{\partial t}[(1-\varepsilon^o)\rho_s + (1-\varepsilon_d)(\varepsilon^o - \varepsilon)\rho_f] = \rho_f \frac{d\sigma}{dt} \tag{4}$$

Species Balance Equation for the Brownian Fines

$$\frac{\partial}{\partial t}(\varepsilon_l c_f) + u_l \frac{\partial}{\partial z}(\varepsilon_l c_f) = D_l \frac{\partial^2}{\partial z^2}(\varepsilon_l c_f) - N_f + r^c_{\text{det}} \tag{5}$$

Species Balance Equation for the κ-Size Aggregate

$$\frac{\partial}{\partial t}(\varepsilon_l c_{a,k}) + u_l \frac{\partial}{\partial z}(\varepsilon_l c_{a,k}) = D_l \frac{\partial^2}{\partial z^2}(\varepsilon_l c_{a,k}) - N_{a,k}\gamma_{a,k} + r^c_{\text{det},a,k} + r^h_{\text{det},a,k}(1-\gamma_{a,k}) \tag{6}$$

Momentum Balance Equations for the Dispersed Gas and Continuous Fluid Phases

$$\frac{\partial}{\partial t}(\rho_g \varepsilon_g u_g) + u_g \frac{\partial}{\partial z}(\rho_g \varepsilon_g u_g) = \varepsilon_g \mu^e_g \frac{\partial^2 u_g}{\partial z^2} - \varepsilon_g \frac{\partial P}{\partial z} + \varepsilon_g \rho_g g - F_{gl} - F_{gs} \tag{7}$$

$$\frac{\partial}{\partial t}(\rho_l \varepsilon_l u_l) + u_l \frac{\partial}{\partial z}(\rho_l \varepsilon_l u_l) = \varepsilon_l \mu^e_l \frac{\partial^2 u_l}{\partial z^2} - \varepsilon_l \frac{\partial P}{\partial z} + \varepsilon_l \rho_l g + \frac{\varepsilon\eta_e - \varepsilon_l}{\varepsilon_g}[F_{gl} + F_{gs}] - F_{ls} \tag{8}$$

Filtration Equation for the Brownian Fines

$$\frac{d\sigma_f}{dt} = N_f - \sum_{k=2}^{\max} \frac{dn_k}{dt} v_f k - r^c_{\text{det}}(\sigma_f) \tag{9}$$

Generation and Filtration Equation for the κ-Size Aggregate

$$\frac{d\sigma_{a,k}}{dt} = \frac{dn_k}{dt} v_f k + N_{a,k}\gamma_{a,k} - r^c_{\text{det},a,k}(\sigma_{a,k}) - r^h_{\text{det},a,k}(1-\gamma_{a,k}) \tag{10}$$

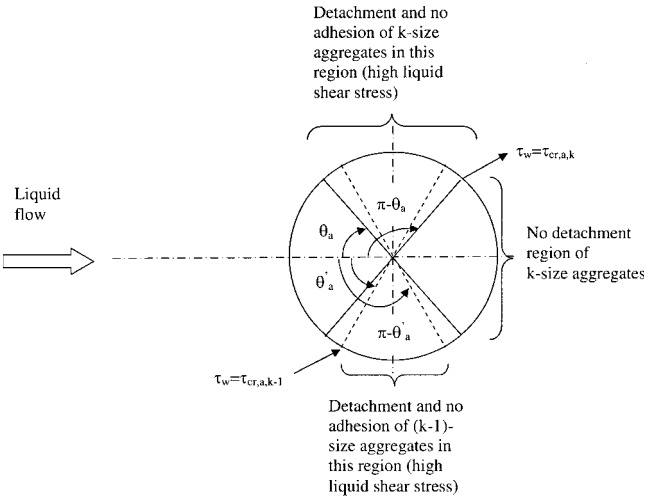

Figure 1. Portions of a collector where particle adhesion, aggregate generation, and detachment occur.

Global Filtration Equation

$$\frac{d\sigma}{dt} = \frac{d\sigma_f}{dt} + \sum_{k=2}^{\max} \frac{d\sigma_{a,k}}{dt} \tag{11}$$

It should be noted that in the case of non-Brownian aggregates, in the previous general model, the rate of reentrainment of colloidal aggregates is negligible ($r^c_{\text{det,a,k}} = 0$). In the above model, P stands for pressure; ε_α, ρ_α, and u_α represent, respectively, the holdup, the density, and the longitudinal (interstitial) velocity of phase α (gas or fluid phases); whereas the subscripts s and f refer to the solid phase (or collectors) and fines, respectively. $F_{\alpha-\beta}$ represents the interfacial drag force per unit reactor volume exerted at the interface between mutually interacting α and β phases (gas, fluid, and solid phases). The fluid-phase effective viscosity μ^e_α, which arises from the combination of the viscous and the pseudoturbulence stress tensors, is formulated as proposed by Dankworth et al.[34] In addition, g is the acceleration arising from gravity, ε is the local porosity at time t, ε^o is the initial *clean* bed porosity, ε_d is the deposit porosity of fines and aggregates, c_α is the local volumetric concentration of Brownian particles or aggregates, N_ξ ($\xi = f$ or $\xi = a, k$) is the local filtration rate of Brownian particles or aggregates, and $\gamma_{a,k}$ represents the fraction of the collector surface area not available for the κ-size aggregate detachment. Note that in the formulation of the momentum balance equations, the capillary pressure between liquid and gas phases is neglected.

The fraction of the collector surface area not available for the detachment of κ-size aggregate particles ($\gamma_{a,k}$) corresponds to the regions where the shear stress acting on the collector is lower than the critical shear stress (Figure 1).[17] In the case of Brownian aggregates the detachment by hydrodynamic mechanism is not possible because critical shear stress is very high and all of the particle surface area is not available for detachment ($\gamma = 1$).

The filtration rate for the κ-size aggregate, which represents the volume of κ-size aggregate deposited per unit reactor volume, is the algebraic sum of the κ-size aggregate accumulation rate, the deposition rate, and the colloidal and hydrodynamic reentrainment rates (Eq. 10). The filtration rate for Brownian particles is the algebraic sum of the deposition rate, the accumulation rate of aggregates, and the colloidal reentrainment rate (Eq. 9).

Deposition rate

The logarithmic law of Iwasaki[35] was used to express the dependency of the deposition rate on the concentration of Brownian particles or aggregates and the superficial liquid velocity:

$$N = \lambda c v_l \tag{12}$$

The filter coefficient λ is the probability for a Brownian particle or a detached aggregate to be captured as it travels a unit distance through the bed. The form of the filter coefficient is dictated by the nature of the capture phenomena in play and by the amount of capture as bed plugging proceeds. Only the deposition under favorable conditions for surface interactions was considered (attractive double-layer force). The influence of the gas phase on the deposition process of Brownian particles and aggregates was neglected. Both monolayer and multilayer depositions were considered for Brownian particles and only monolayer deposition in the case of the detached aggregates. In this work, the expressions developed by Rajagopalan and Tien[36] and Tien et al.[37] were used to calculate the filter coefficient for monolayer ($\sigma \leq \sigma_{cr}$) and multilayer deposition ($\sigma > \sigma_{cr}$), respectively. Rajagopalan and Tien[36] estimated single-collector efficiency and finally the filter coefficient for monolayer deposition by numerically solving the trajectory equation for a non-Brownian spherical fine particle in the vicinity of a spherical collector. The trajectory equation was developed by formulating a force balance for a suspended particle that included the effects arising from gravity, fluid drag, van der Waals interactions, and increased viscous resistance to particle motion near the collector surface. The flow in the porous medium was represented by Happel's sphere-in-cell model in which the packed bed is assumed to consist of spherical grains, each of which is encapsulated by a spherical liquid envelope. The diameter of the envelope is chosen such that the porosity of the unit formed by the grain and the liquid envelope is equal to the overall bed porosity. Combining the trajectory analysis results with the contribution of the Brownian diffusion yielded the following expression for the monolayer filter coefficient ($\sigma \leq \sigma_{cr}$) in terms of dimensionless parameters, N_{L}, N_R, N_G, and N_{Pe}, representing the mechanisms for particle–media interactions:

$$\lambda = \lambda^o = \frac{3}{2}(1-\varepsilon^o)^{1/3}\frac{\eta^o}{d_p^o} \tag{13}$$

where

$$\eta^o = A_s^o(1-\varepsilon^o)^{2/3}N_R^{15/8}N_{\mathrm{L}}^{1/8} + 0.00338A_s^o(1-\varepsilon^o)^{2/3}N_G^{6/5}N_R^{-2/5} + 4(A_s^o)^{1/3}(1-\varepsilon^o)^{2/3}(N_{\mathrm{Pe}})^{-2/3} \tag{14}$$

$$A_s^o = \frac{2(1-p^5)}{w} \qquad p = (1-\varepsilon^o)^{1/3}$$
$$w = 2 - 3p + 3p^5 - 2p^6 \tag{15}$$

Here, A_s^o is a porosity-dependent parameter accounting for the effects of neighboring collectors, N_R is a dimensionless number describing the effect of particle and collector sizes, N_G accounts for gravity effects, N_{L} reflects van der Waals interactions, and N_{Pe} expresses the role of Brownian diffusion. The mechanism of interception is accounted for by the A_s^o and N_R factors. The first term in Eq. 14 characterizes the collection that occurs arising from the van der Waals attraction force; the second term characterizes the collection that occurs as a result of gravitational sedimentation; and the third term expresses the role of Brownian diffusion. For multilayer deposition ($\sigma > \sigma_{cr}$), Tien et al.[37] developed the following expression for the filter coefficient:

$$\frac{\lambda}{\lambda^o} = B_1\frac{A_s}{A_s^o}\left[1+\frac{\sigma}{(1-\varepsilon^o)(1-\varepsilon_d)}\right]^{17/24} + B_2\frac{A_s}{A_s^o}\left[1+\frac{\sigma}{(1-\varepsilon^o)(1-\varepsilon_d)}\right]^{4.4/3} + B_3\left(\frac{A_s}{A_s^o}\right)^{1/3}\left[1+\frac{\sigma}{(1-\varepsilon^o)(1-\varepsilon_d)}\right]^{4/9} \tag{16}$$

where

$$\frac{A_s}{A_s^o} = \left[\frac{1-(1-\varepsilon)^{5/3}}{1-(1-\varepsilon^o)^{5/3}}\right] \times \left[\frac{2-3(1-\varepsilon^o)^{1/3}+3(1-\varepsilon^o)^{5/3}-2(1-\varepsilon^o)^2}{2-3(1-\varepsilon)^{1/3}+3(1-\varepsilon)^{5/3}-2(1-\varepsilon)^2}\right] \tag{17}$$

In the case of Brownian particle deposition, the critical specific deposit σ_{cr} corresponds to the amount of Brownian particles required for completing a monolayer having a coating porosity ε_d. σ_{cr} is calculated assuming sphere-in cell model configuration[38]:

$$\sigma_{cr} = \left[\left(\frac{d_p^o + 2d_f}{d_p^o}\right)^3 - 1\right](1-\varepsilon_d)(1-\varepsilon^o) \tag{18}$$

Detachment rate

For colloidally induced release (Brownian particles/aggregates), in the absence of an energy barrier, the detachment rate is based on the assumption that the rate-limiting step is the diffusion of detached colloids across the boundary layer between collector surfaces and liquid bulk:[28]

$$r_{\mathrm{det},i}^c = \alpha_{\mathrm{det},i}^c \bar{a}(1-\varepsilon)\eta_e d_i \sigma_i \tag{19}$$

where $\alpha_{\mathrm{det,i}}^{\mathrm{c}}$ designates the Brownian fines detachment ($i = f$) or the κ-size aggregate detachment ($i = a, k$). $\alpha_{\mathrm{det},i}^{\mathrm{c}}$ is the first-order release rate coefficient reflecting diffusive trans-

port of detached colloids across the diffusion boundary layer and depend on the colloid diffusion coefficient and the boundary layer thickness:[28]

$$\alpha^{c}_{\mathrm{det},i} = \frac{D_{\mathrm{BM},i}}{\delta^{2}_{bl,i}} \tag{20}$$

For non-Brownian aggregates, the rate of hydrodynamic particle reentrainment was considered to be proportional to the difference between the wall shear stress and the critical shear stress[22,23]

$$r^{h}_{\mathrm{det},a,k} = \alpha^{h}_{\mathrm{det},a,k}\bar{a}(1-\varepsilon)\eta_e(\tau_w - \tau_{cr,a,k})\frac{1}{\rho_f} \quad \text{for} \quad \tau_w > \tau_{cr,a,k} \tag{21}$$

$$r^{h}_{\mathrm{det},a,k} = 0 \qquad \text{for} \quad \tau_w < \tau_{cr,a,k} \tag{22}$$

Physically, Eqs. 21 and 22 indicate that, to initiate the release of aggregates, the wall shear stress as a result of liquid (and indirectly gas) flows should be greater than a *critical shear stress*. Implicit in this formulation is the assumption that the critical shear stress is an indicator of the strength of intraparticle bonds binding the aggregates to the pore wall. Critical shear stress was estimated for the condition of equilibrium between the forces acting on an attached aggregate along the tangential direction:[17]

$$\tau_{cr,a,k} = \frac{k_f \frac{6(1-\varepsilon^o)}{d_p^o}\frac{\mathrm{Ha}}{12\delta^2}}{2.551\pi d_{a,k}} \tag{23}$$

The shear stress acting on the collector was estimated using Happel's model:

$$\tau_w = 3\mu_l \frac{A_s}{d_p} u_l \tag{24}$$

where

$$A_s = \frac{2(1-p^5)}{w} \qquad p = (1-\varepsilon)^{1/3}$$
$$w = 2 - 3p + 3p^5 - 2p^6 \tag{25}$$

Aggregation rate

Particle aggregation can be described by the rate at which a certain size aggregate is being formed by smaller aggregates less the rate at which the aggregate combines to form a larger aggregate (neglecting aggregate breakup). This is given by the discrete population balance equations of von Smoluchowski[21]:

$$\frac{dn_k}{dt} = \frac{1}{2}\alpha \sum_{i+j=k} \beta_{ij} n_i n_j - n_k \alpha \sum_{i=1}^{\max} \beta_{ik} n_i \quad k = 2,3,\ldots,\max \tag{26}$$

where α is the fractional collision efficiency; β_{ij} is the rate at which particles of volume v_i and v_j collide; n_i is the number density of particles with volume v_i; i, j, k refer to particle size class indices; and max refers to a maximum size class. The first summation is over the sets of sizes that, when added, produce a κ-size aggregate. The second summation reflects the loss of κ-size aggregates as they combine with all other aggregates sizes to form larger aggregates.

According to the von Smoluchowski model, the colloidal particles in the flow field are assumed to follow the fluid streamlines and collide with each other when the distance between the streamlines is less than the sum of the particle radii. However, during a collision between two particles, the particles experience hydrodynamic and repulsive or attractive forces. Taking these forces into account, a factor is introduced, called the orthokinetic collision efficiency α that represents the ratio of actual aggregation rate to von Smoluchowski's aggregation rate. Collision efficiency is a complex function of the surface properties of the particles, the structure of the aggregates or the diameter of the aggregates, hydrodynamic effects, and the prevailing colloidal forces.[39]

The collision frequency function β_{ij} reflects the physical environment, such as temperature, viscosity, shear stress, and aggregation size. It is generally accepted that there are three mechanisms that cause particle collision: Brownian motion or perikinetic aggregation, differential settling, and liquid shear or orthokinetic aggregation. The collision frequency function arising from Brownian motion is[40]

$$\beta_{ij,\mathrm{BR}} = \frac{2\kappa_{\mathrm{B}}T}{3\mu_l}\left(\frac{1}{r_i} + \frac{1}{r_j}\right)(r_i + r_j) \tag{27}$$

where r_i is the aggregate radius, T is absolute temperature, μ_l is the liquid viscosity, and $\boldsymbol{\kappa}_{\mathrm{B}}$ is Boltzmann's constant.

Differential settling occurs when larger aggregates settle more rapidly than smaller aggregates and particles. The terminal velocity of settling particles and aggregates is assumed to follow Stokes's law. Considering differential settling rates and the rectilinear collision model, the rate constant is described by[41]

$$\beta_{ij,\mathrm{DS}} = \frac{\pi g(\rho_p - \rho_l)}{72\mu_l}(d_i + d_j)^3 |d_i - d_j| \tag{28}$$

where ρ_p and ρ_l are the aggregate and the liquid densities, respectively.

For liquid shear-induced aggregation, the most widely accepted form of the collision frequency function is that based on a purely rectilinear model. That is, particle trajectories at some distance from the particle under observation are considered to continue along the same path and not be influenced be the flow field surrounding the observed particle. A "collision sphere" can be conceptualized as a sphere with its origin at a particle center. The radius of the collision sphere is $r_i + r_j$, the radii of the two particles that may collide. If the center of the second particle passes within the collision sphere, a collision will occur between the two particles. The collision frequency function for rectilinear model is given by[42]

$$\beta_{ij,\mathrm{SH}} = \frac{1}{6}(d_i + d_j)^3 G_m \tag{29}$$

where G_m is the mean velocity gradient in the liquid (s^{-1}).

The aggregates consisting of solid particles can be treated using a fractal dimension. Thus, the radius $r_{a,k}$ of a size class

κ aggregate (consisting of k primary particle of radius $r_l = r_f$) can be expressed as[54]

$$r_{a,k} = r_1(k)^{1/D_f} \tag{30}$$

where D_f is the fractal dimension, which defines the relationship between particle size and density. Fractal dimension takes values between 1 and 3. Coalescing sphere models, which include the original von Smoluchowski equation, assume that D_f is equal to 3.

Interfacial drag forces

The assumption of bed partial wetting entrains that the gas-phase drag will have contributions arising from the effects located at the gas–liquid (F_{gl}) and gas–solid (F_{gs}) interfaces. Similarly, the resultant of the forces exerted on the liquid phase involves two components: (1) the drag force, F_{ls}, experienced by the liquid as a result of the shear stress near the liquid–solid boundary; and (2) the gas–liquid interfacial drag resulting from the slip between fluids, F_{gl}. Assuming trickle flow regime, the double slit model provides satisfactory approximations for the liquid–solid, gas–solid, and gas–liquid drag forces[43]:

$$F_{ls} = \eta_e \left\{ \frac{\mathrm{E}_1}{36} C_w^2 \frac{\bar{a}^2 (1-\varepsilon)^2 \mu_l \eta_e}{\varepsilon_l^3} + \frac{\mathrm{E}_2}{6} (1+\psi_{gl}) C_{wi} \frac{\bar{a}(1-\varepsilon)}{\varepsilon_l^3} \rho_l |v_l| \right\} v_l \varepsilon_l \tag{31}$$

$$F_{gs} = (1-\eta_e) \left\{ \frac{\mathrm{E}_1}{36} C_w^2 \frac{\bar{a}^2 (1-\varepsilon)^2 \mu_g}{\varepsilon^3} + \frac{\mathrm{E}_2}{6} C_{wi} \frac{\bar{a}(1-\varepsilon)}{\varepsilon^3} \rho_g |v_g| \right\} v_g \varepsilon \tag{32}$$

$$F_{gl} = \eta_e \left\{ \frac{\mathrm{E}_1}{36} C_w^2 \frac{\bar{a}^2 (1-\varepsilon)^2 \mu_g}{(\varepsilon - \varepsilon_l/\eta_e)^2 \varepsilon_g} + \frac{\mathrm{E}_2}{6} C_{wi} (1+\psi_{gl}) \times \frac{\bar{a}(1-\varepsilon)\rho_g}{(\varepsilon - \varepsilon_l/\eta_e)^2 \varepsilon_g} |v_g - (\varepsilon - \varepsilon_l/\eta_e) u^*| \right\} \times \left[v_g - (\varepsilon - \varepsilon_l/\eta_e) u^* \right] \varepsilon_g \tag{33}$$

where the effective surface area can be expressed as the summation of the surface area of the porous medium and the surface area of the Brownian particles (we considered the specific solid deposit being formed only by Brownian particles):

$$\bar{a} = \frac{N_c \zeta \pi d_p^2(t) + N_c \partial N_{\mathrm{B}} \left[\zeta \pi d_f^2 - A_\Delta(t) \right]}{N_c \frac{\pi}{6} (d_p^0)^3 + N_{\mathrm{B}} \frac{\pi}{6} d_f^3} \tag{34}$$

The first term in the numerator of Eq. 34 reflects the area of the porous medium (that is, the collectors) and the second, the area of the particles and agglomerates that becomes available for particle interception. With the progress of deposition, the solid–liquid surface area becomes altered by two opposing phenomena[44]: (1) an increase in surface area through addition of the area of the captured particles and aggregates exposed to streamline flow and (2) a loss of area A_Δ resulting from the *shadow effect*[31] (the shadow effect refers to the fact that once a particle is captured by a collector certain parts of the collector surface near the deposited particle are not accessible to approaching particles). Not all of the original media collector or the deposited particles and aggregates are available for momentum transfer because of packing structure, fracturing, or cul-de-sac formation.

The increase in the collector diameter was calculated as a function of the specific deposit, assuming a sphere-in-cell model configuration:[38]

$$d_p(t) = d_p^o \sqrt[3]{1 + \frac{\sigma}{(1-\varepsilon_d)(1-\varepsilon^o)}} \tag{35}$$

Numerical Implementation

To make the Euler–Euler model (Eqs. 1–11, 26, and 27) solvable, boundary and initial conditions need to be specified for the system in the trickle flow regime. It is assumed that there is an inlet of gas and liquid at the top of the reactor and corresponding outlets at its bottom. The pressure, the concentration of Brownian particles, the liquid and gas holdups, and the gas and liquid interstitial velocities are specified at the inlet. To solve the partial differential equations, we discretized in space and solved the resulting set of ordinary differential equations. The spatial discretization is performed using the standard cell-centered finite-difference scheme. The GEAR integration method for stiff differential equations was used to integrate the time derivatives.

The aggregation model stability was examined by the number or mass conservation during aggregation modeling, which can be represented by a mass conservation factor that is the ratio of the total number of primary particles for each aggregate size class to the initial primary particle number concentration:

$$\text{Mass conservation factor} = \frac{\sum_{k=1}^{\max} k(n_k)_t}{(n_1)_{t=0}} \tag{36}$$

To describe the aggregation process a maximum size class (k) of 25 was used. Although it would be desirable to have an unlimited size class such that the aggregate growth would be unbounded, computationally this is not possible. So, this maximum size class was limited.

Transient flow simulations in a clean bed are first performed until the (pressure, velocity, and holdup) flow fields reach steady state. Under these circumstances, the conservation equations (Eqs. 1–3, 7, and 8) are solved in the absence of fines in the liquid phase. Starting from these solutions, transient simulations with fines-containing liquid are then resumed by solving Eqs. 1–11 and 26. Simulations are carried out on a Pentium IV processor running at 2500 MHz. The relative error tolerance for the time integration process in the present simulations is set at 10^{-6} for each time step.

Results and Discussion

Experimental verification

In a previous work, we validated a filtration model for two-phase flow coupled only with the deposition process of

Table 1. Model Parameters

Material Property	Value
Liquid: Straight run gas oil	
Viscosity	0.24×10^{-3} Pa · s
Density	610 kg/m^3
Surface tension	7.8×10^{-3} N/m
Superficial velocity	0.006 m/s
Gas: Hydrogen	
Superficial velocity	0.028 m/s
Fine particles: Kaolinite	
Average diameter	1–2 μm
Density	2000 kg/m^3
Porosity of deposit layer	0.8[11]
Influent concentration	1.0 g/L
Packing: Spherical catalyst particles	
Diameter	0.003 m
Bed porosity	0.37
Ergun constants	$E_1 = 195$, $E_2 = 1.75$
Geometry of fixed-bed reactor	
Diameter	0.051 m
Height	0.9 m
Temperature	573 K
Pressure	10 MPa
Coefficient of sliding friction	$k_f = 3.79 \times 10^{-6}$ m[26]
Hamaker constant	$Ha = 1.4 \times 10^{-20}$ J
Hydrodynamic release rate coefficient	$\alpha^h_{det} = 1.4 \times 10^{-8}$ kg N^{-1} s^{-1}

fines.[14] However, there is no single work in the literature about two-phase flow in which coupling between fine particles deposition, aggregation, and release processes in trickle-bed reactors has been attempted. For such reasons, no experimental data can be procured for validation of this new approach for conducting filtration. Therefore, we will illustrate in this investigation the theoretical promises, if any, that this novel method could hold.

Estimation of model parameters

To make the model solvable, the Ergun constants (E_1 and E_2), the liquid axial dispersion coefficient (D_l), the external wetting efficiency (η_e), the surface-area parameter (ζ), the hydrodynamic release rate coefficient (α^h_{det}), the fractional collision efficiency (α), and the fractal dimension (D_f) need to be specified. The Ergun single-phase flow parameters can either be set by measurements of single-phase pressure drops[45] or estimated from literature correlations.[46] The wetting efficiency was evaluated using the comprehensive neural network correlation developed by Larachi et al.[47] The extent of back-mixing in the liquid phase is quantified in terms of an axial dispersion coefficient, which is evaluated using a recent comprehensive Bodenstein number correlation.[48] The geometrical parameter ζ, which represents the percentage of a single-particle surface area truly available for momentum transfer, has been included to account for this loss of area. According to the simulation results, roughly 55% of the surface area is available for momentum transfer and thus for particle capture.[44,49] The hydrodynamic release rate coefficient α^h_{det} was taken from plume test experiments of Arulanandan et al.[23] This value of hydrodynamic release rate coefficient, obtained under relatively unconstrained flow tests, is in good agreement with that used by Sen et al.[30] to characterize fines transport in fixed beds having porosity around 0.3–0.32, which may be thought of as a realistic lower limit threshold for nonconsolidated porous media such as those dealt with in this study. Collision efficiency α ranges between 0.0001 and 13.[41] However, in theory, the collision efficiency approaches unity when colloidal interactions are dominated by deposition as in our case.[50] Even though the fractal dimensions D_f from many different systems are broadly reported between 1.0 and 3.0 (an aggregate fractal dimension of 3.0 implies spherical aggregation),[51] they often fall between 1.7 and 2.85.[52,53] In this work, fractal dimension D_f was varied between 2 and 3.[54]

Simulation

Capture, aggregation, release, and migration of Brownian particles and aggregates in two-phase flow porous media sys-

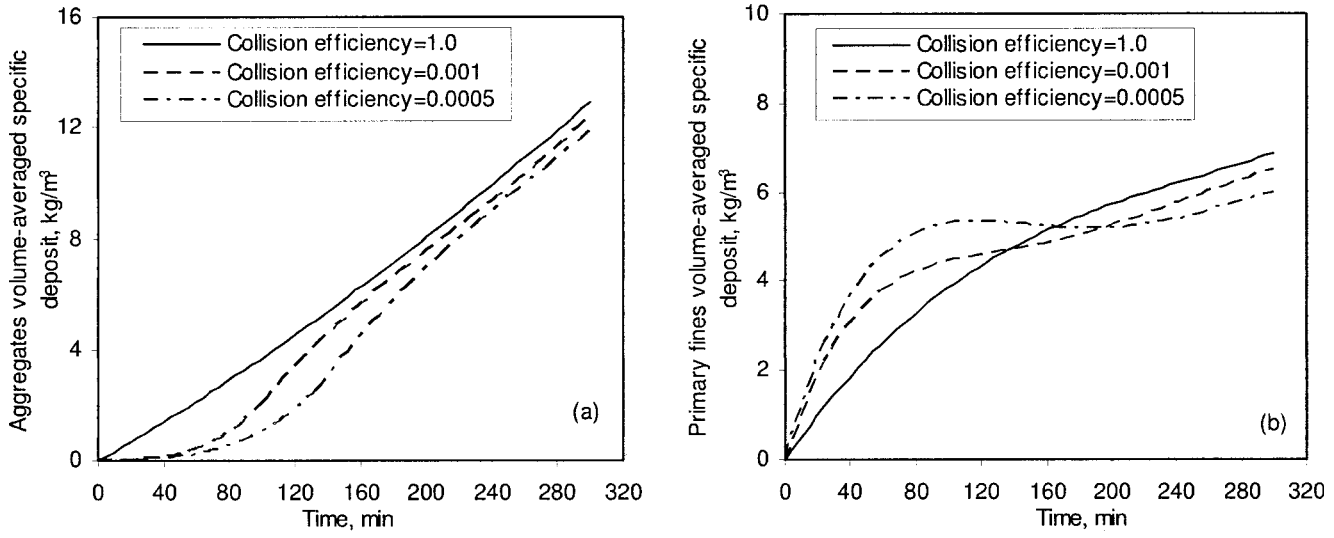

Figure 2. Impact of collision efficiency on the aggregates and fines average specific solid deposit.

$d_f = 2$ μm, $D_f = 2.0$, max = 15.

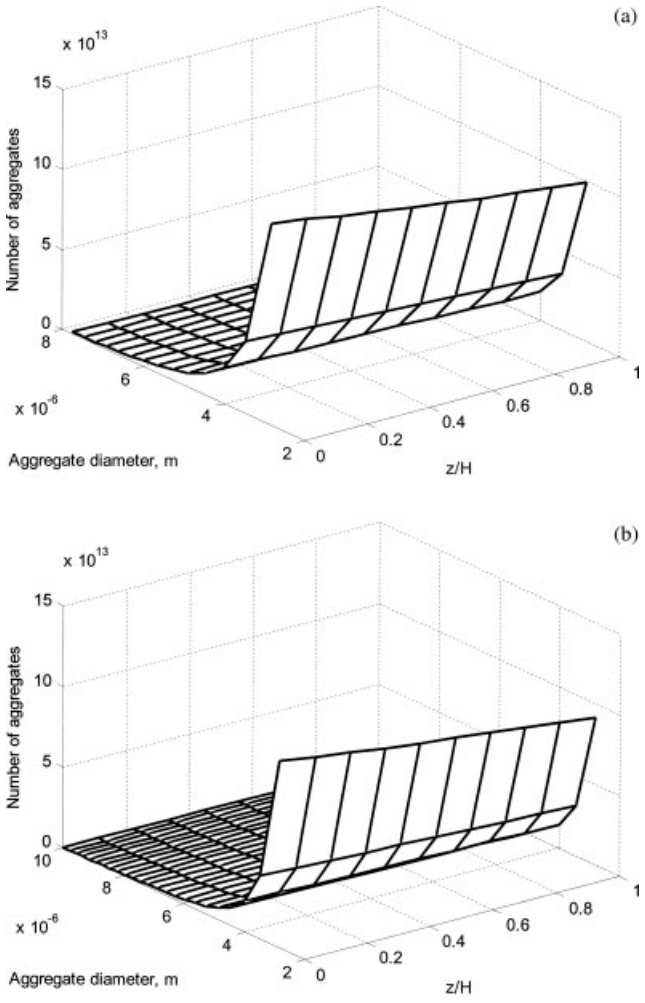

Figure 3. Variation of number of aggregates of different dimensions along axial coordinate.

$d_f = 2$ μm, $\alpha = 1.0$, $D_f = 2.0$, $t = 167$ min: (a) max = 15; (b) max = 25.

tems are complex so that flow field imaging of the transient phenomena accompanying fluid flow, fine particles deposition, aggregation, and fine particles and aggregates release is not trivial and has not yet been experimentally attempted. It is proposed here to test the model potentiality through simulations of different experimental configurations by solving the transport equations for trickle-bed reactors experiencing plugging by particle deposition, aggregation, and detachment. Plugging tests at high temperature and pressure are simulated using gas oil as the liquid phase (containing kaolinite fine particles) and hydrogen as the gas phase. Spherical (γ-alumina) catalytic particles are used as collectors. The simulated conditions are listed in Table1 and coincide with typical hydrotreating conditions.[55,56]

The first set of simulations concerns Brownian fine particles deposition/aggregation/release for different values of collision efficiency (Figure 2). The model is sufficiently sensitive to collision efficiency at the beginning of the plugging process. There is a noticeable decrease in the aggregates volume-average specific deposit with decreasing collision efficiency that is coherent and also mirrored by the increased fines volume-average specific deposit. At high collision efficiency the rate of Brownian particle agglomeration is elevated and the aggregates volume-average specific deposit increases. If the collision efficiency is <0.001, slow aggregation can be expected. At long term, given that plugging is a slow (large timescale) unsteady-state phenomenon, the collision efficiency has only a moderate influence on the aggregation process. Because the collision efficiency approaches unity when colloidal interactions are dominated by deposition,[50] the following simulations were undertaken for these conditions.

The second set of simulations concerns Brownian fine particles deposition/aggregation/release for different values of maximum size class of the aggregates. With the increase of the maximum size class of the aggregates, for a given fractal dimension and collision efficiency, the number of non-Brownian aggregates able to be detached by hydrodynamic

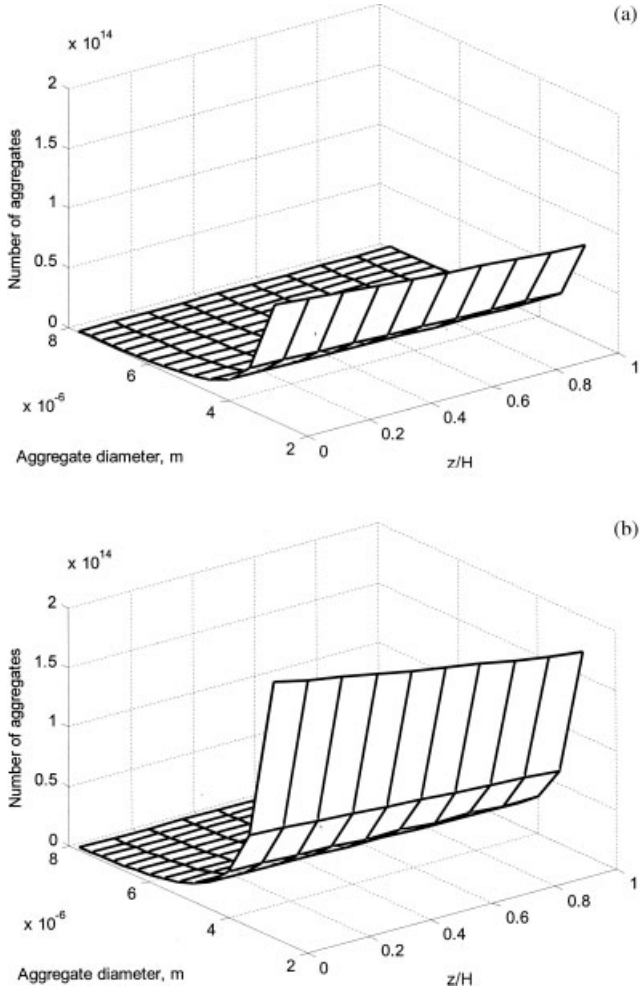

Figure 4. Variation of number of aggregates of different dimensions along axial coordinate.

$d_f = 2$ μm, $\alpha = 1.0$, $D_f = 2.0$, max = 15: (a) $t = 133$ min; (b) $t = 267$ min.

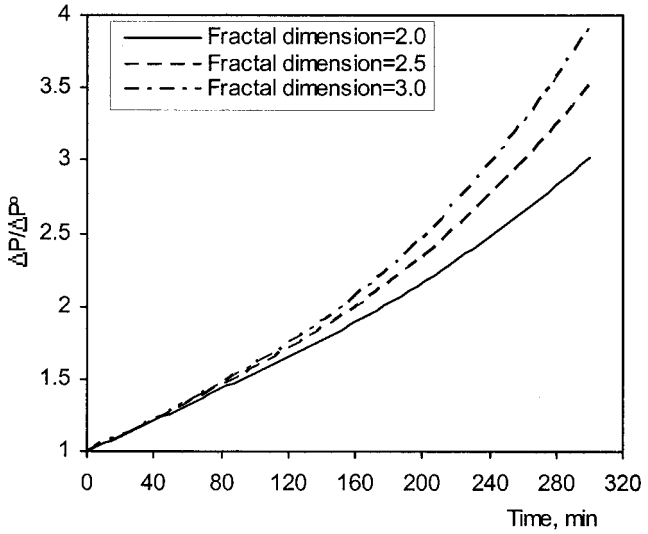

Figure 5. Impact of aggregate fractal dimension on transient behavior of two-phase pressure drop.

$d_f = 2$ μm, $\alpha = 1.0$, max = 15.

forces increases (Figure 3). However, the total volume-average solid deposit and two-phase pressure drop do not change with the value of maximum size class of the aggregates. This is because the deposition rate of the detached non-Brownian aggregates is higher than the detachment rate and there is an equilibrium between the non-Brownian aggregates deposition and reentrainment and, consequently, the aggregates volume-average solid deposit is not influenced by the hydrodynamic detachment. Although it would be desirable to have an unlimited size class such that the aggregate growth would be unbounded, computationally this is not possible. In the following simulations the maximum size of the aggregates (k) is limited to 15 to have a reasonable computational time.

Figure 4 shows the variation of the number of aggregates of different diameter with the axial distance at $t = 133$ min and $t = 267$ min. The figure shows that there is a significant accumulation of the aggregates within the 2.8–3.5 μm size range at any time because the number of the primary Brownian particles transported from the bulk liquid to the surface of the collector increases in time. Also, this figure shows that the number of large non-Brownian aggregates prone to detach by hydrodynamic forces is very low.

When a liquid suspension passes through a bed, some of the Brownian fines are retained by the bed (the deposition being caused by diffusion, interception, gravitational collection, and collection arising from surface forces) and two-phase pressure drop (ΔP) increases compared to that for the clean bed without fines (ΔP^o) (see Figure 5). The major change resulting from fine particles deposition involves bed porosity and therefore the increase of two-phase pressure drop is the result of a decrease in bed porosity. Figure 5 shows that the two-phase pressure drop ratio is higher for higher values of fractal dimension. With the increase of fractal dimension the aggregates volume-average solid deposit increases (Figure 6a) and, consequently, the primary Brownian fines volume-average solid deposit decreases (Figure 6b). At higher fractal dimension, the rate of colloidally induced release of primary Brownian deposited particles decreases as a result of lower primary Brownian fines volume-average solid deposit and the result is a higher total volume-average deposit (Figure 6c) and a higher two-phase pressure drop (Figure 5). On the other hand, a smaller fractal dimension for a given collision efficiency results in a larger aggregate size and a larger number of non-Brownian aggregates able to be detached by hydrodynamic forces. However, as mentioned earlier, the deposition rate of the detached non-Brownian aggregates is higher than the detachment rate and there is an equilibrium between the non-Brownian aggregates deposition and reentrainment and therefore the aggregates volume-average solid deposit is not influenced by the hydrodynamic detachment.

Figure 7 shows the effect of the primary Brownian fines diameter on the fines and aggregates volume-average specific deposit. In the case of a lower diameter of primary Brownian particles, even if the majority of aggregates is colloidal (Figure 8) and the rate of colloidally induced release of the aggregates is very high, the fines and aggregates volume-average specific deposits are higher for $d_f = 2$ μm (Figure 7). The number of primary Brownian particles transported from the bulk liquid to the surface of the collector and the number of the Brownian particles found in the aggregates are higher for $d_f = 1$ μm (Figure 8). However, this is not reflected in higher values for fines deposition rate and generation rate of the aggregates, stated as $m^3_{solid}/m^3_{reactor}s$. The deposition rate and the generation rate of the aggregates are higher in the case $d_f = 2$ μm, yielding higher fines- and aggregates-specific deposits at the same filtration time. As a consequence, the decrease in the bed porosity is much higher for $d_f = 2$ μm and therefore the increase of two-phase pressure drop is most significant (Figure 9).

Conclusions

A Euler–Euler fluid dynamic model—based on the volume average mass, momentum, and species balance equations, filtration equations for the Brownian particles and aggregates, and the discrete population balance equations for the agglomeration of particles—was proposed for the description of two-phase flow and deposition/aggregation/release of Brownian fine solids in high-pressure/temperature trickle-bed reactors. Both monolayer and multilayer depositions were considered for Brownian particles and only monolayer deposition in the case of the detached aggregates. The release of fine particles and aggregates from the collector surface was supposed to be induced by the colloidal forces in the case of Brownian particles/aggregates or by the hydrodynamic forces in the case of non-Brownian aggregates. Brownian particle aggregation was described by the rate at which a certain size aggregate is being formed by smaller aggregates less the rate at which the aggregate combines to form a larger aggregate.

The plugging with fine particles and aggregates was analyzed in terms of transient volume-average specific deposit and two-phase pressure drop buildup. The following conclusions can be drawn from the simulation results:

- The two-phase pressure drop ratio is higher for higher values of aggregate fractal dimension.

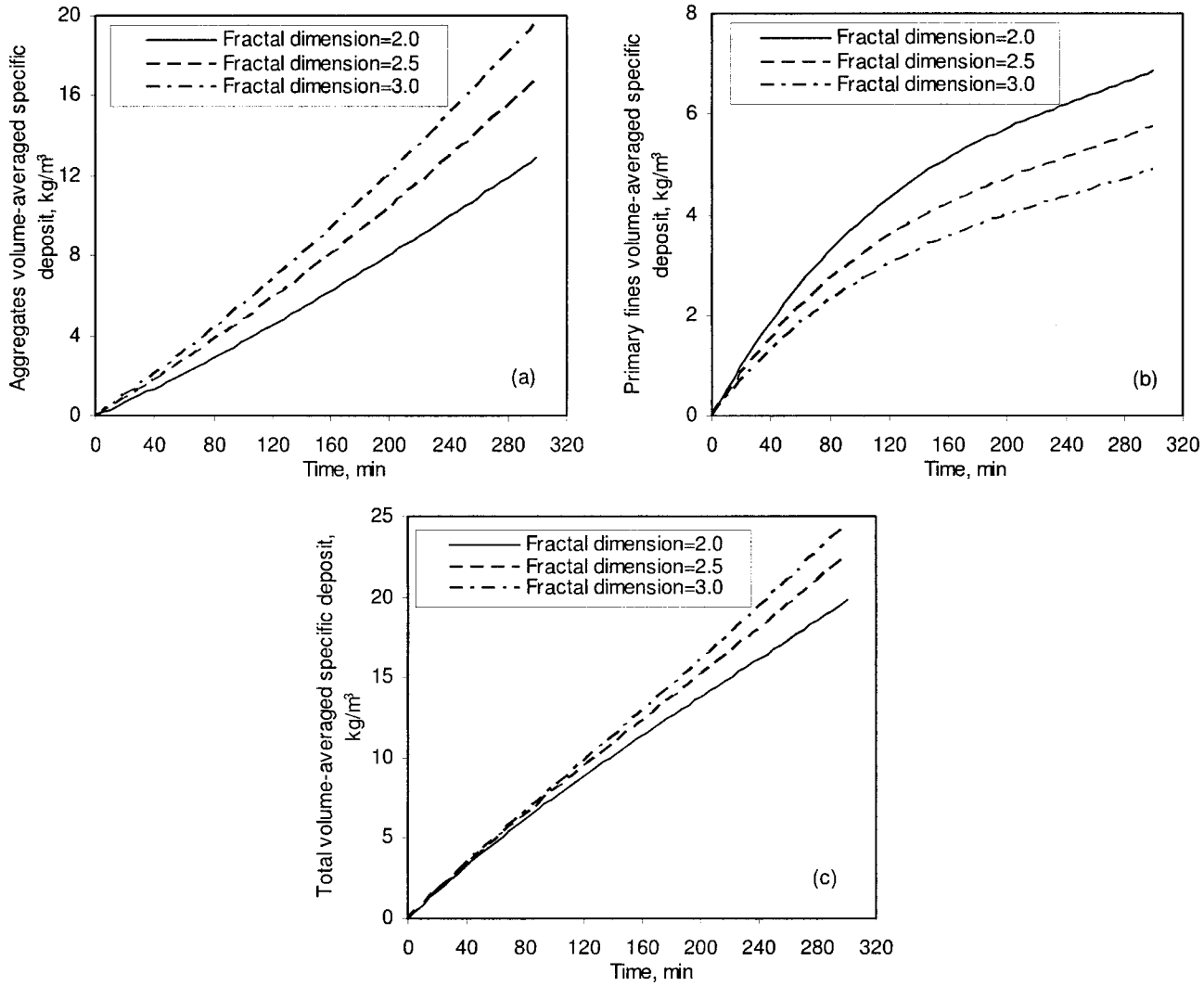

Figure 6. Effect of aggregate fractal dimension on transient behavior of aggregates, fines, and total average specific solid deposit.

$d_f = 2$ μm, $\alpha = 1.0$, max = 15.

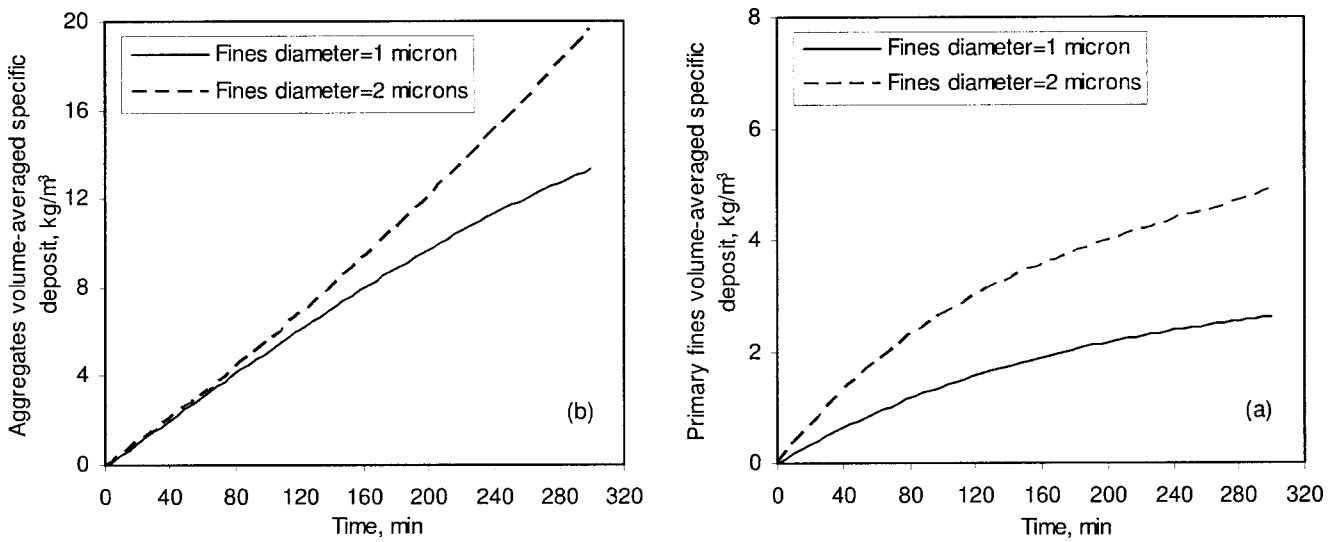

Figure 7. Impact of primary Brownian particles diameter on aggregates and fines average specific solid deposit.

$D_f = 3.0$, $\alpha = 1.0$, max = 15.

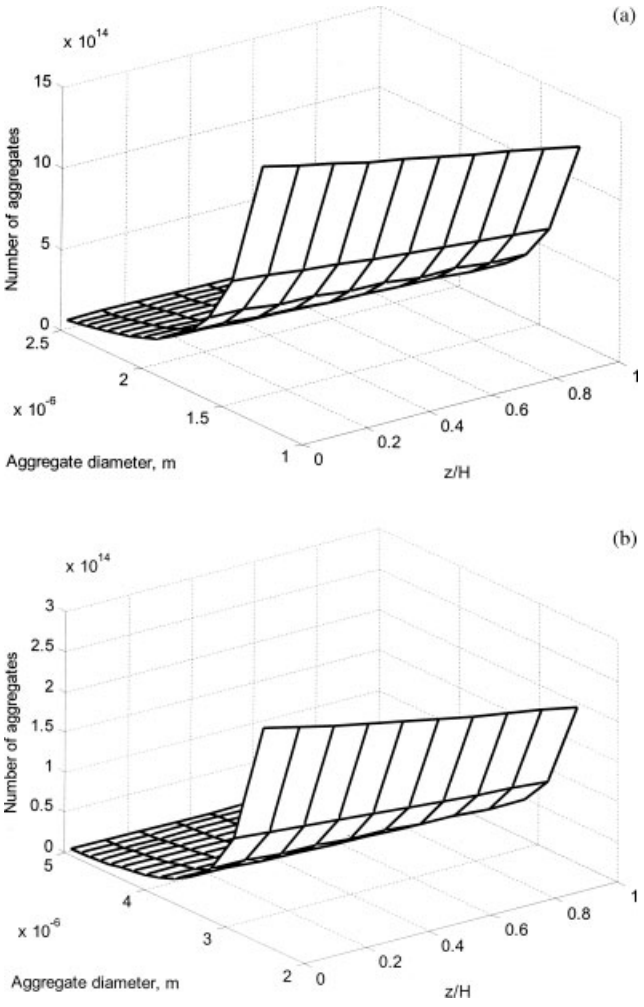

Figure 8. Variation of number of aggregates of different dimensions along axial coordinate.

$\alpha = 1.0, D_f = 3.0$, max = 15, $t = 300$ min: (a) $d_f = 1$ μm; (b) $d_f = 2$ μm.

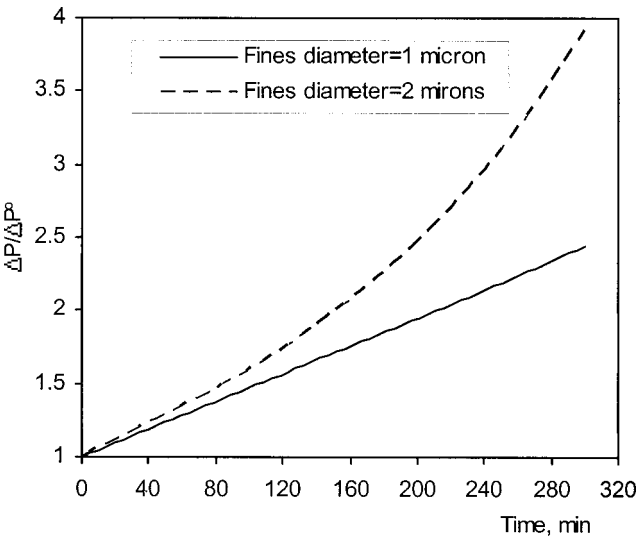

Figure 9. Two-phase pressure drop ratio vs. time at different diameter values of fine particles.

$D_f = 3.0$, $\alpha = 1.0$, max = 15.

- At long term the collision efficiency has only a moderate influence on the aggregation process.
- The number of large non-Brownian aggregates prone to detach by hydrodynamic forces is very low.
- There is an equilibrium between the non-Brownian aggregates deposition and reentrainment so the aggregates volume-average solid deposit is not influenced by hydrodynamic detachment.
- Aggregation of primary Brownian particles with a low diameter results in a majority of colloidal aggregates.

Acknowledgments

Financial support from the Natural Sciences and Engineering Research Council of Canada through its Strategic Program Grants is acknowledged.

Notation

M_{M1}, M_{M2} = effective specific surface area (surface of the particles/volume of the solid phase), m^2/m_s^3

A_Δ = collector area loss,

$$= A_\Delta = \tfrac{1}{2}\left[\frac{d_p(t)}{2}\right]^2\left[2\sqrt{3}\frac{d_f}{d_p(t)} - \sin\left(2\sqrt{3}\frac{d_f}{d_p(t)}\right)\right], \text{m}^2$$

B_1 = coefficient in Eq. (16),

$$B_1 = [(1-\varepsilon^o)^{2/3}/\eta^o]A_s^o N_{\text{L}}^{1/8} N_R^{15/8}$$

B_2 = coefficient in Eq. (16),

$$B_2 = 3.376 \times 10^{-3}\frac{(1-\varepsilon^o)^{2/3}}{\eta^o}A_s^o N_G^{1.2} N_R^{-0.4}$$

B_3 = coefficient in Eq. (16),

$$B_3 = \frac{4\sqrt[3]{A_s^o}N_{\text{Pe}}^{-2/3}}{\eta^o}$$

$c_{a,k}$ = κ-size aggregate concentration (liquid volume basis)
c_f = fine volumetric concentration (liquid volume basis)
$d_{a,k}$ = κ-size aggregate diameter, m
d_c = column diameter, m
d_f = fine particle diameter, m
d_p = effective particle diameter

$$d_p(t) = d_p^o\sqrt[3]{1 + [\sigma/(1-\varepsilon_d)(1-\varepsilon^o)]}, \text{m}$$

$D_{BM,i}$ = Brownian diffusion coefficient,

$$D_{\text{BM},i} = \frac{2\kappa_{\text{B}}\text{T}}{6\pi\mu_l d_i}\,(i = f \text{ or } a,k)$$

D_f = fractal dimension
D_l = axial dispersion coefficient in liquid phase, m^2/s
E_1, E_2 = Ergun constants
F_{gl} = gas–liquid drag force, N/m^3
F_{gs} = gas–solid drag force, N/m^3
F_{ls} = liquid–solid drag force, N/m^3
g = gravity acceleration, m/s^2
H = bed height, m
Ha = Hamaker constant, J
k = particle size class index
κ_B = Boltzmann's constant, J/K
k_F = coefficient of sliding friction, m
max = maximum size class of the aggregates

n_1 = number density of primary Brownian particles
n_k = number density of κ-size aggregate
$N_{a,k}$ = deposition rate of κ-size aggregate (reactor volume basis), s^{-1}
N_c = number of collectors in grid cell volume v,

$$N_c = [6v/\pi(d_p^o)^3](1-\varepsilon^o)$$

N_f = deposition rate of Brownian particles (reactor volume basis), s^{-1}
N_B = number of trapped Brownian fines in grid cell volume v,

$$N_f = [(6v/\pi d_f^3)](\varepsilon^o-\varepsilon)(1-\varepsilon_d)$$

∂N_B = number of peripheral Brownian fines per collector,

$$\partial N_f = 4\beta(1-\varepsilon_d)\left[\frac{d_p(t)}{d_f}\right]^2$$

N_G = gravitational dimensionless group,

$$N_G = \frac{(\rho_f-\rho_l)d_f^2 g}{18\pi\mu_f v_l}, \text{where } j = f \;\&\; a,k$$

N_L = London–van der Waals dimensionless group,

$$N_L = \frac{4Ha}{9\pi\mu_l d_f^2 v_l}, \text{where } j = f \;\&\; a,k$$

N_{Pe} = Brownian diffusion group

$$N_{Pe} = \frac{d_p(t)v_l}{D_{BM}}$$

N_R = interception dimensionless group

$$N_R = \frac{d_j}{d_p^o}, \text{where } j = f \;\&\; a,k$$

N_ξ = local filtration rate of Brownian particles or aggregates, where $\xi = f$ or $\xi = a, k$
P = pressure, Pa
R = constant of ideal gas, J kg^{-1} K^{-1}
T = temperature, K
u_α = average interstitial velocity of α-phase, m/s
v = grid cell volume, m^3
v_f = volume of primary Brownian particles, m^3
v_α = α-phase superficial velocity, m/s

Greek letters

α = collision efficiency,
α_{det}^c = colloidal first-order release rate coefficient, s^{-1}
α_{det}^h = hydrodynamic release rate coefficient, kg N^{-1} s^{-1}
β = collector cross-sectional fraction,

$$\beta = 1 - \frac{1}{2}\left[\frac{d_p^o}{d_p(t)}\right]^2\left[1-\frac{d_p(t)}{d_p(t)+2d_f}\right]$$

β_{ij} = collision frequency function
$\gamma_{a,k}$ = fraction of the collector surface area not available for the κ-size aggregates detachment[17]; $\gamma_{a,k} = \sin\theta_a = \tau_{cr,a,k}/\tau_w$
$\gamma_{a,k-1}$ = fraction of the collector surface area not available for the (κ − 1)-size aggregates detachment[17]; $\gamma_{a,k-1} = \sin\theta_a = \tau_{cr,a,k-1}/\tau_w$
δ = separation distance between the fine particle and the collector plane[57]; $\delta = 4\times10^{-10}$
δ_{bl} = thickness of the boundary layer around a single spherical colloid, $\delta_{bl} = r_p(D_{BM}/u_l r_p)^{1/3}$
ε = bed porosity
$<\varepsilon>$ = bed volume-average porosity
ε_d = porosity of deposits
ε_g = gas holdup
ε_l = liquid holdup
η = collector efficiency
η_e = wetting efficiency
λ = filter coefficient, m^{-1}
λ_o = clean filter coefficient, m^{-1}
μ_α = α-phase dynamic viscosity, kg m^{-1} s^{-1}
μ_α^e = α-phase effective viscosity (combination of bulk and shear terms), kg m^{-1} s^{-1}
ρ_α = density of α-phase, kg/m^3
σ = global specific deposit,

$$\sigma = \sum_{k-2}^{\max}\sigma_{a,k} + \sigma_f = (\varepsilon^o-\varepsilon)(1-\varepsilon_d)$$

$<\sigma>$ = bed volume-average specific deposit,

$$\langle\sigma\rangle = H^{-1}\int_0^H \sigma(t)dz$$

$\sigma_{a,k}$ = κ-size aggregate specific deposit (reactor volume basis)
σ_f = Brownian particles specific deposit (reactor volume basis)
τ_w = shear stress on the collector plan, N/m^2
ζ = surface-area parameter
ψ_{gl} = gas–liquid interaction factor

Subscripts

M_{M1}, M_{M2} = κ-size aggregate
f = Brownian fine
g = gas phase
l = liquid phase
s = solid phase

Superscript

M_{M1}, M_{M2} = clean bed state

Literature Cited

1. Shafi R, Hutchings GJ. Hydrodesulfurization of hindered dibenzothiophenes: An overview. *Catal Today*. 2000;59:423–442.
2. Reinhoudt HR, Boons CHM, van Langeveld AD, van Veen JAR, Sie ST, Moulijn JA. On the difference between gas- and liquid-phase hydrotreating test reactions. *Appl Catal A Gen*. 2001;207:25–36.
3. Speight JG. *The Desulfurization of Heavy Oil and Residua*. 2nd Edition. New York: Marcel Dekker; 2000.
4. Chen J, Ring Z, Dabros T. Modeling and simulation of a fixed-bed pilot-plant hydrotreater. *Ind Eng Chem Res*. 2001;40:3294–3300.
5. Narayan R, Coury JR, Masliyah JH, Gray MR. Particle capture and plugging in packed-bed reactors. *Ind Eng Chem Res*. 1997;36:4620–4627.
6. Wang S, Chung KH, Masliyah JH, Gray MR. Deposition of fine particles in packed beds at hydrotreating conditions: Role of surface chemistry. *Ind Eng Chem Res*. 1999;38:4878–4888.
7. Gray MR, Srinivasan N, Masliyah JH. Pressure buildup in gas–liquid flow through packed beds due to deposition of fine particles. *Can J Chem Eng*. 2002;80:346–354.
8. Hahn MW, O'Melia CR. Deposition and reentrainment of Brownian particles in porous media under unfavorable chemical conditions: Some concepts and applications. *Environ Sci Technol*. 2004;38:210–220.
9. Kim J, Tobiason JE. Particles in filter effluent: The roles of deposition and detachment. *Environ Sci Technol*. 2004;38:6132–6138.
10. Bai R, Tien C. Transient behaviour of particle deposition in granular media under various surface interactions. *Colloids Surf A Physicochem Eng Aspects*. 2000;165:95–114.
11. Tien C. *Granular Filtration of Aerosols and Hydrosols*. Stoneham, MA: Butterworths; 1989.
12. Chan EW, Chung KH, Veljkovic M, Liu JK. Hydrodynamics and fines capture in packed-bed hydrotreaters. Proceedings of the International Petroleum and Petrochemical Technology Symposium, Beijing, China, September; 1995:15–17.

13. Wang S, Chung KH, Gray MR. Role of hydrotreating products in deposition of fine particles in reactors. *Fuel*. 2001;80:1079–1085.
14. Iliuta I, Larachi F, Grandjean BPA. Fines deposition dynamics in trickle flow reactors. *AIChE J*. 2003;49:485–495.
15. Iliuta I, Larachi F. Fines deposition dynamics in packed-bed bubble reactors. *Ind Eng Chem Res*. 2003;42:2441–2449.
16. Iliuta I, Larachi F. Onset of pulsing in gas–liquid trickle bed filtration. *Chem Eng Sci*. 2004;59:1199–1211.
17. Iliuta I, Larachi F. Stretching operational life of trickle-bed filters by liquid-induced pulse flow. *AIChE J*. 2005;51:2034–2047.
18. Iliuta I, Ring Z, Larachi F. Simulating simultaneous fines deposition under calalytic hydrodesulfurization in hydrotreating trickle beds—Does bed plugging affect HDS performance? *Chem Eng Sci*. 2006;61:1321–1333.
19. Ortiz-Arroyo A, Larachi F. Lagrange–Euler–Euler CFD approach for modeling deep bed filtration in trickle flow reactors. *Sep Purif Technol*. 2005;41:155–172.
20. Elimelech M, Gregory J, Jia X, Williams RA. *Particle Deposition and Aggregation: Measurement, Modelling and Simulation*. Boston, MA: Butterworth-Heinemann Ltd.; 1995.
21. von Smoluchowski M. Versuch einer Mathematischen Theorie der Koagulationskinetik Kolloider Losungen. *Z Phys Chem.* 1917;92: 129–168.
22. Khilar KC, Fogler HS. *Migration of Fines in Porous Media*. Dordrecht, The Netherlands: Kluwer Academic; 1998.
23. Arulanandan K, Longanathan P, Krone KB. Pore and eroding fluid influences on surface erosion of soil. *J Geotech Eng Div ASCE*. 1975;101:51–65.
24. Ginn T, Amirtharajah A, Karr PR. Effects of particle detachment in granular-media filtration. *J Am Water Works Assoc*. 1992;84:66–76.
25. Moran MC, Moran DC, Cushing RS, Lawler DF. Particle behavior in deep-bed filtration: Part 2—Particle detachment. *J Am Water Works Assoc*. 1993;85:82–90.
26. Bai R, Tien C. Particle detachment in deep bed filtration. *J Colloid Interface Sci*. 1997;186:307–317.
27. Gruesbeck C, Collins RE. Entrainment and deposition of fines particles in porous media. *Soc Pet Eng J*. 1982;22:847–856.
28. Ryan JN, Gschwend PM. Effects of ionic strength and flow rate on colloid release: Relating kinetics to intersurface potential energy. *J Colloid Interface Sci*. 1994;164:21–34.
29. Khilar KC, Fogler HS. Water sensitivity of sandstones. *Soc Pet Eng J*. 1983;23:55–64.
30. Sen TK, Nalwaya N, Khilar KC. Colloid-associated contaminant transport in porous media: 2. Mathematical modeling. *AIChE J*. 2002;48:2375–2385.
31. Tien C, Payatakes AC. Advances in deep bed filtration. *AIChE J*. 1979;25:737–759.
32. Choo CU, Tien C. Simulation of hydrosol deposition in granular media. *AIChE J*. 1995;41:1426–1433.
33. Whitaker S. The transport equations for multi-phase systems. *Chem Eng Sci*. 1973;28:139–147.
34. Dankworth DC, Kevrekidis IG, Sundaresan S. Dynamics of pulsing in trickle beds. *AIChE J*. 1990;36:605–621.
35. Iwasaki T. Some notes on sand filtration. *J Am Water Works Assoc*. 1937;29:1591–1602.
36. Rajagopalan R, Tien C. Trajectory analysis of deep-bed filtration with the sphere-in-cell porous media model. *AIChE J*. 1976;22:523–533.
37. Tien C, Turian RM, Pendse H. Simulation of the dynamic behavior of deep bed filters. *AIChE J*. 1979;25:385–404.
38. Choo CU, Tien C. Analysis of the transient behavior of deep-bed filtration. *J Colloid Interface Sci*. 1995;169:13–33.
39. Burban PY, Lick W, Lick J. The flocculation of fine-grained sediments in estuarine waters. *J Geophys Res*. 1989;94:8323–8331.
40. Friedlander SJ. *Smoke, Dust, and Haze*. New York: Wiley–Interscience; 1972.
41. Gardner KH, Theis TL, Young TC. Colloid aggregation: Numerical solution and measurements. *Colloids Surf A Physicochem Eng Aspects*. 1998;141:237–252.
42. Gardner KH, Theis TL. A unified kinetic model for particle aggregation. *J Colloid Interface Sci*. 1996;180:162–173.
43. Iliuta I, Grandjean BPA, Larachi F. New mechanistic film model for pressure drop and liquid holdup in trickle flow reactors. *Chem Eng Sci*. 2002;57:3359–3371.
44. Stephan EA, Chase GG. Development of volume-average theory for deep-bed filtration. *AIChE J*. 2000;46:1918–1926.
45. Holub RA, Dudukovic MP, Ramachandran PA. A phenomenological model of pressure drop, liquid holdup and flow regime transition in gas–liquid trickle flow. *Chem Eng Sci*. 1992;47:2343–2348.
46. Iliuta I, Larachi F, Grandjean BPA. Pressure drop and liquid holdup in trickle flow reactors: Improved Ergun constants and slip correlations for the slit model. *Ind Eng Chem Res*. 1998;37:4542–4550.
47. Larachi F, Belfares L, Grandjean BPA, Prediction of liquid–solid wetting efficiency in trickle flow reactors. *Int Commun Heat Mass Transfer*. 2001;28:595–603.
48. Piché S, Larachi F, Iliuta I, Grandjean BPA. Improving predictions of liquid back-mixing in trickle-bed reactors using a neural network approach. *J Chem Technol Biotechnol*. 2002;77:989–999.
49. Ortiz-Arroyo A, Larachi F, Grandjean BPA, Roy S. Modeling and simulation of clogging in packed-bed reactors with non-aqueous media using CFD. *AIChE J*. 2002;48:1596–1609.
50. Huang CH, Pan JR, Huang S. Collision efficiency of algae and kaolin in depth filters: The effect of surface properties of particles. *Water Res*. 1999;33:1278–1286.
51. Jiang Q, Logan BE. Fractal dimension of aggregates determined from steady state size distributions. *Environ Sci Technol*. 1991;25: 2031–2038.
52. Wiesner MR. Kinetics of aggregate formation in rapid mix. *Water Res*. 1992;26:379–387.
53. Sterling MC, Bonner JS, Ernest ANS, Page CA, Autenrieth RL. Application of fractal flocculation and vertical transport model to aquatic sol-sediment systems. *Water Res*. 2005;39:1818–1830.
54. Kim J-W, Kramer TA. Improved models for fractal colloidal agglomeration: Computationally efficient algorithms. *Colloids Surf A Physicochem Eng Aspects*. 2005;253:33–49.
55. Broderick DH, Gates BC. Hydrogenolysis and hydrogenation of dibenzothiophene catalysed by sulfided CoO-MoO_3/γ-Al_2O_3: The reaction kinetics. *AIChE J*. 1981;27:663–672.
56. Korsten H, Hoffman U. Three-phase reactor model for hydrotreating in pilot trickle-bed reactor. *AIChE J*. 1996;42:1350–1360.
57. Visser J. Particle adhesion and removal—A review. *Particle Sci Technol*. 1995;13:169–179.

Manuscript received Oct. 7, 2005, revision received Apr. 18, 2006, and final revision received Sept. 14, 2006.